2018

Experimental Study of Frost Accretion on Hydrophilic and Hydrophobic Substrates under Forced Convection Conditions

Valter Nascimento
Federal University of Parana, Brazil, vsallesjr@gmail.com

Felipe Loyola
POLO Labs, Federal University of Santa Catarina, Brazil, felipe.loyola@polo.ufsc.br

Christian Hermes
POLO Labs, Federal University of Santa Catarina, Brazil, hermes@polo.ufsc.br

Rodrigo P. Cardoso
UFPR, Brazil, rodrigo.perito@ufpr.br

Andrew Sommers
Dept. of Mechanical and Manufacturing Engineering, Miami University, Oxford, OH 45056, sommerad@miamioh.edu

Experimental Study of Frost Accretion on Hydrophilic and Hydrophobic Substrates under Forced Convection Conditions

Valter S. NASCIMENTO Jr. [1], Felipe R. LOYOLA [2], Christian J. L. HERMES [2,*]
Rodrigo P. CARDOSO [1], Andrew D. SOMMERS [3],

[1] Post-Graduation Program in Materials Science and Engineering, Federal University of Paraná
81531-990, Curitiba, PR, Brazil

[2] POLO Research Laboratories, Department of Mechanical Engineering, Federal University of Santa Catarina
88040-900, Florianópolis, SC, Brazil

[3] Department of Mechanical and Manufacturing Engineering, Miami University
56 Garland Hall, 650 East High Street, Oxford, OH 45056 USA

[*] Corresponding Author: hermes@polo.ufsc.br

ABSTRACT

The present study is aimed at investigating, by means of an experimental approach, the effect of surface wettability on the frost accretion over horizontal flat surfaces under forced convection conditions. A purpose-built closed-loop wind-tunnel facility was especially designed and constructed to provide a strict control of the psychrometric conditions at the entrance of the test section, and also of the plate surface temperature. An image acquisition system was used to measure the thickness of the frost layer over time. A dataset comprised of more than 800 experimental data points spanning different surface temperatures (from -20 to -10°C) and air temperatures (from 5 to 16C°), with the modified Jakob number ranging from 1.05 to 2.10, and contact angles ranging from 60° to 123° was gathered and used to investigate both the individual and the simultaneous effects of key heat and mass transfer parameters on the frost growth rate. A first-principles modelling approach was used together with the experimental data obtained in-house to come out with a semi-empirical fully-algebraic expression for the frost thickness as a function of the time, the supercooling degree, and the surface contact angle. It was found that the proposed correlation was able to predict most of the experimental data points (>90%) for the frost thickness within ±15% error bounds. Insights on the early and delayed nucleation where also obtained from the analysis of the experimental data.

1. INTRODUCTION

Surface frosting is likely to take place in several engineering applications, from aviation to HVAC-R systems, impacting not only on equipment performance, but also affecting aspects such as safety and cost. Under frosting conditions, refrigerator evaporators tend to be rather inefficient because of the requirement for periodic defrosting (Silva and Hermes, 2018). Moreover, because the frost layer acts as an additional thermal resistance, the cooling capacity of the evaporator tends to decrease with ongoing frost growth, and thus the compressor needs to run longer cycles to achieve the desired cooling effect (Ribeiro and Hermes, 2018).

Due to its importance to the refrigeration industry, research on frost nucleation, growth and densification phenomena have been steadily increased in the past decades. In their recent review paper, Song and Dang (2018) demonstrated that the fundamental frost formation research has been historically (from the 1960s to 2010s) focused on frost morphology, growth rate, properties (density and thermal conductivity), whereas applied research has been carried out aiming at evaporator frosting and defrosting processes, leading not only to better and safer products (know-how), but also expanding the boundaries of the knowledge (know-why).

The influence of the (micro- and mesoscopic) surface characteristics, particularly the wettability on the thermophysical (macroscopic) properties of frost, especially the porosity has gained attention of the community in

the past decade (Kim et al., 2017), as surface coatings (either hydrophilic or hydrophobic) are sometimes used to mitigate frost build-up and/or improve drainage during the defrost cycle. It is likely that the idea of using surface coatings to mitigate evaporator frosting probably derived from the air conditioning practice of using different fin materials to aid drainage of condensation. In the early 2000s, Jhee et al. (2002) conducted frosting experiments for evaporators covered with a hydrophobic coating, showing that the heat transfer performance improved when compared to the baseline. Results of this kind have triggered a steadily increase in the number of publications focused on frost formation on hydrophilic and hydrophobic substrates (Lee at al., 2004; Liu et al., 2006; Wu et al., 2007; and Piucco et al., 2008).

Studies of the effect of surface wettability on the frost growth and densification processes proliferate in the current decade, most of them aimed at the solidification of water droplets. For instance, Farhadi et al. (2011) studied the performance of frost formation retardation on various hydrophobic surfaces, concluding that the durability of the coating is a problem to be considered, and also that the hydrophobic effect of the surfaces is significantly lower at low temperatures. Kim and Lee (2011) investigated the effects of freezing of water on the surfaces of fins previously treated to obtain different contact angles: hydrophilic 2.5°, baseline 75° and hydrophobic 142°, observing that the hydrophobic fin delayed the frost formation while the hydrophilic one had a thinner and denser frost thickness. Wang et al. (2015) studied a hydrophobic coating that provided a contact angle of 147°, showing a delayed frost growth by 60 min if compared to an untreated aluminum surface. Rahimi et al. (2015) analyzed the initial stages (5 to 10 min) of frost growth on aluminum surfaces with contact angles from 80 to 120°, reporting a slow frost build-up on hydrophobic surfaces, and the opposite behavior on hydrophilic ones. Sommers et al. (2016) evaluated the time-evolution of frost density in three different substrates with contact angles: 45.3°, 81.9° and 158.9°, noticing a reduction in frost density by 40% for the hydrophobic surface, whereas for the hydrophilic surface produced a reduction by 25% in frost density. In follow-up studies by the same group, semi-empirical correlations for the frost density (Sommers et al., 2017) and thickness (Sommers et al., 2018) in hydrophilic and hydrophobic surfaces were presented and validated for a wide span of contact angles under free convection conditions.

In the present paper, the effect of surface wettability on the frost accretion over horizontal flat surfaces is studied under forced convection conditions. A purpose-built closed-loop wind-tunnel facility was especially designed and constructed to provide a strict control of the psychrometric conditions at the entrance of the test section, and also of the plate surface temperature. The first-principles model proposed by Hermes et al. (2018) and used by Sommers et al. (2018) was used together with the experimental data obtained in-house to come out with a semi-empirical fully-algebraic expression for the frost thickness as a function of the time, the supercooling degree and the contact angle. It was found that the proposed correlation was able to predict most of the experimental data points (>90%) for the frost thickness within ±15% error bounds. Insights on the early and delayed nucleation where also obtained from the analysis of the experimental data.

2. EXPERIMENTAL WORK

2.1 Experimental setup

The experiments were carried out by means of a horizontal closed-loop wind-tunnel facility, depicted in Fig. 1, which provides a strict control of the surface temperature and the air conditions (temperature, humidity and velocity). The wind-tunnel walls are made of 50-mm thick EPS (expanded polystyrene) plates sandwiched between 20-mm thick plastic liners to provide structural resistance. The air-loop is comprised of two straight sections and two return bends, all with a 200 x 200 mm cross section. One side contains the ½" and 1" nozzles for air flow measurements, an evaporator coil for cooling and dehumidifying the air stream, and two PID-driven electric heaters, a finned 350-W one for regulating the air temperature and a flat 180-W one immersed in a humidifying tray for controlling the air humidity. A DC fan is also used to set the air velocity at the test section, with air flows ranging from 1 to 20 m³/h. The air flow rate was measured according to the ASHRAE Standard 51 (1999) using a differential pressure transducer ranging from 0 to 125 Pa with an uncertainty of 0.25% full-scale (i.e. 0.35 Pa).

On the other side, there is an EPS-insulated 1.0-m long straight channel, which ensures the proper thermal-fluid-dynamic development, and the test section itself, which is comprised of a PID-controlled thermoelectric device, as illustrated in Fig. 2. The test section is comprised of an aluminum block with a square cross section (L=120 mm x W=60 mm) is connected to the thermoelectric cell located at the outer side of the wind-tunnel walls to facilitate the heat dissipation from the hot ends. The surface under analysis (L=120 mm x W=60 mm) is mounted over the other

end of the aluminum block using thermal grease to enhance thermal contact. A square 22-mm sided triple-layer glass window is located at the test section to allow visualization. A stereoscopic device with a 3 megapixel 10x ocular lens and 0.5x photographic lens camera, was used to take pictures of the frost layer during the test. The illumination was provided by optical fibers. The frost thickness was measured from the images with a ±50 μm uncertainty.

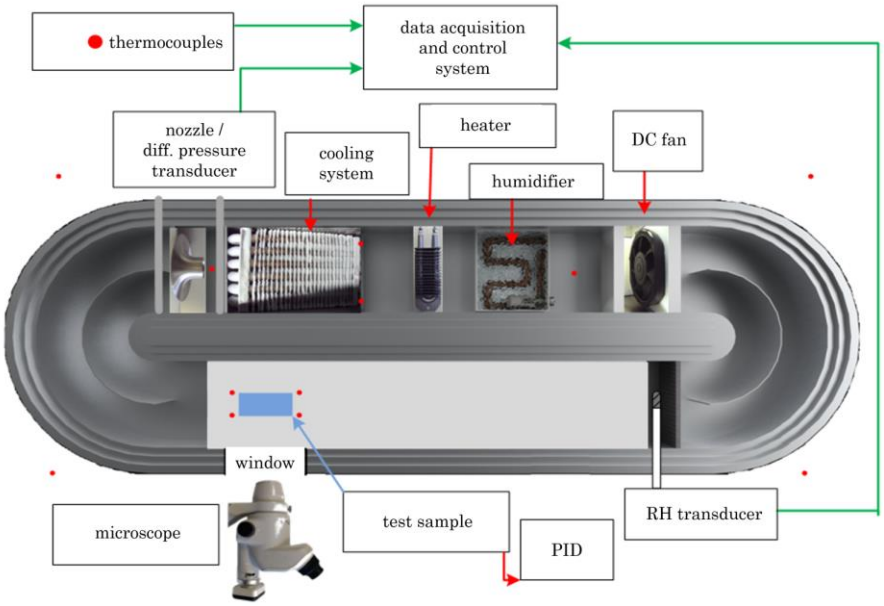

Figure 1: Schematic representation of the closed-loop wind-tunnel facility

A homogenizer was placed at the channel inlet to promote flow laminarization. A capacitive relative humidity transducer (±2% uncertainty) was installed at the channel inlet to control the inflow air humidity by the 180-W heater. In addition, 4 T-type thermocouples (±0.2 K uncertainty) were located at the test section entrance (2) and exit (2) ports, being the upstream ones responsible for controlling the 350-W heater. Additional thermocouples were installed at the plate surface (3 each), at the nozzle (1) and at the surrounding air (1). A data acquisition and control system with 16 channels for temperature measurements, and 16 input and 4 output analogical channels was employed to monitor data and control the facility. The room temperature was kept at 20°C±2°C by an on-off controlled air conditioner. At the end of the test, a scale (±0.01g uncertainty) was used to measure the amount of water deposited on the test surface. The facility operates in a wide span of test conditions, with air temperatures ranging from -5 to 22°C, relative humidity from 30% to 80%, and substrate temperature with a lower limit of -23°C.

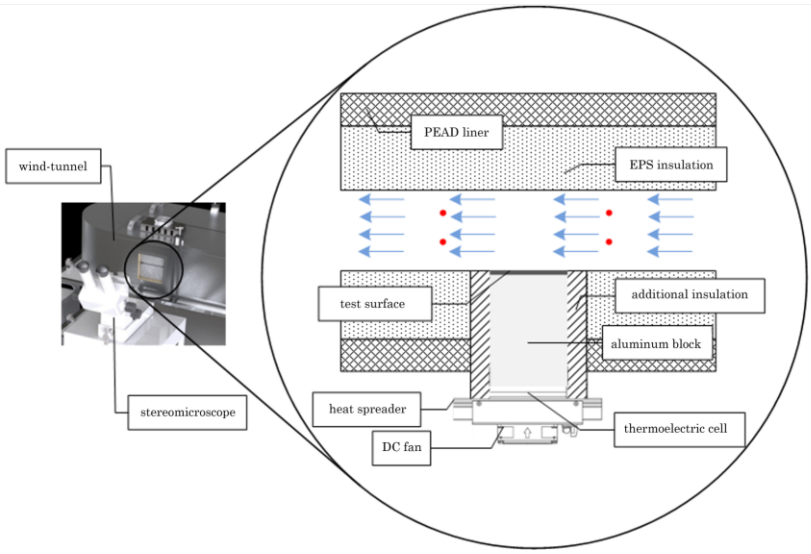

Figure 2. Schematic representation of the test section

2.2 Sampling

The substrates under analysis were W=60 x L=120 mm^2 with a thickness between 6 and 9 mm. Four samples made of aluminum were treated to provide different contact angles, being polished with 1200 grit sandpaper before the treatment. The standard (baseline) surface (S1) was obtained by polishing the aluminum substrate with 1200 grit sandpaper. Sample (S2) was covered with a layer of polytetrafluoroethylene – a stable, low surface energy coating that increases the contact angle. Sample (S3) was polished with 1200 grit and coated with a thin layer of silica by means of the plasma deposition to increase the surface energy, leading to low contact angles. Finally, sample (S4) was obtained by means of a commercial nanometric coating (Nanoclean®) which led to a stable hydrophobic surface. Figure 3 illustrates the surfaces under analysis.

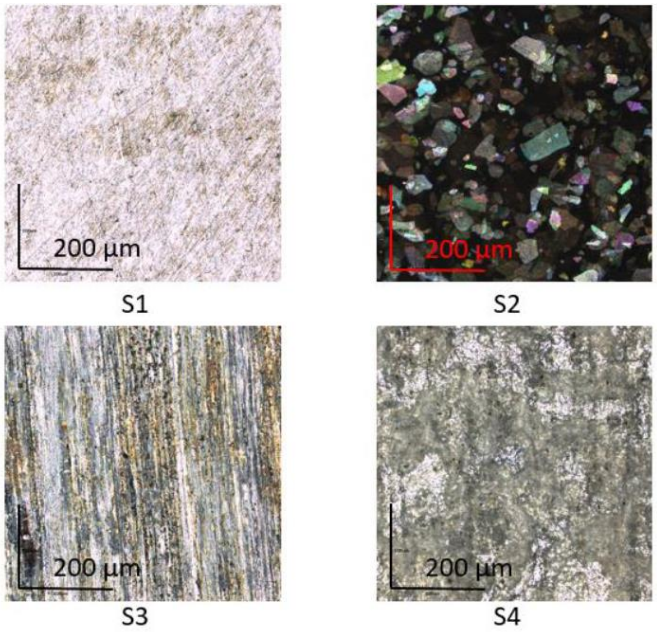

Figure 3: Surfaces under analysis: (S1) Baseline, CA=88°; (S2) Polytetrafluoroethylene, CA=108°; (S3) Hydrophilic, CA=60°; and (S4) Hydrophobic, CA=123° (CA=contact angle)

The characterization of the contact angle (CA) of the test samples was conducted by means of a drop shape analyzer goniometer (±2.5° uncertainty) using acquisition rates of 5 µl/min and 450 µl/min. Twelve measurements were performed for each surface before (6) and after (6) the tests, with the largest and the smallest figures being excluded, and the remaining 10 measurements being averaged and used for measurement uncertainty calculations. Similarly, the roughness of each surface was measured by means of a laser confocal microscope.

2.3 Test Conditions and Procedure

In addition to the contact angle span, ranging from 60° to 123°, the psychrometric conditions of the air stream at the test section inlet and the surface temperature were selected to reproduce the conditions likely to take place in refrigerating appliances. To come out with different frost morphologies, three levels for each the surface (-20, -15 and -10°C) and the air temperatures (5, 10 and 16°C) considering a relative air humidity of 80%, providing a supercooling degree ranging from 10K to 30K, and a modified Jakob number ranging from 1.05 to 2.10. Air velocities spanning 1 to 2 m/s were also considered. In total, 69 runs with 120-min each were conducted.

Prior to the test initialization, the test bench was put to run so that both the air and the surface reach steady-state conditions. To avoid frost accretion on the test surface during the stabilization period, which lasts about 3 hours, the surface was covered with a thin PVC film. Once steady-state is achieved, the plastic film is removed and time counting started. During the tests, the air velocity, temperature and humidity at the entrance of the test section as well as the temperature of the cold plate covered with a sample (S1 to S4) were monitored and recorded. Throughout the experiment, the test section was photographed at every 1-minute, as depicted in Fig. 4. Measurements of the frost thickness were performed at every 10-minutes. For all tests, the dimensions were calibrated using a standard scale.

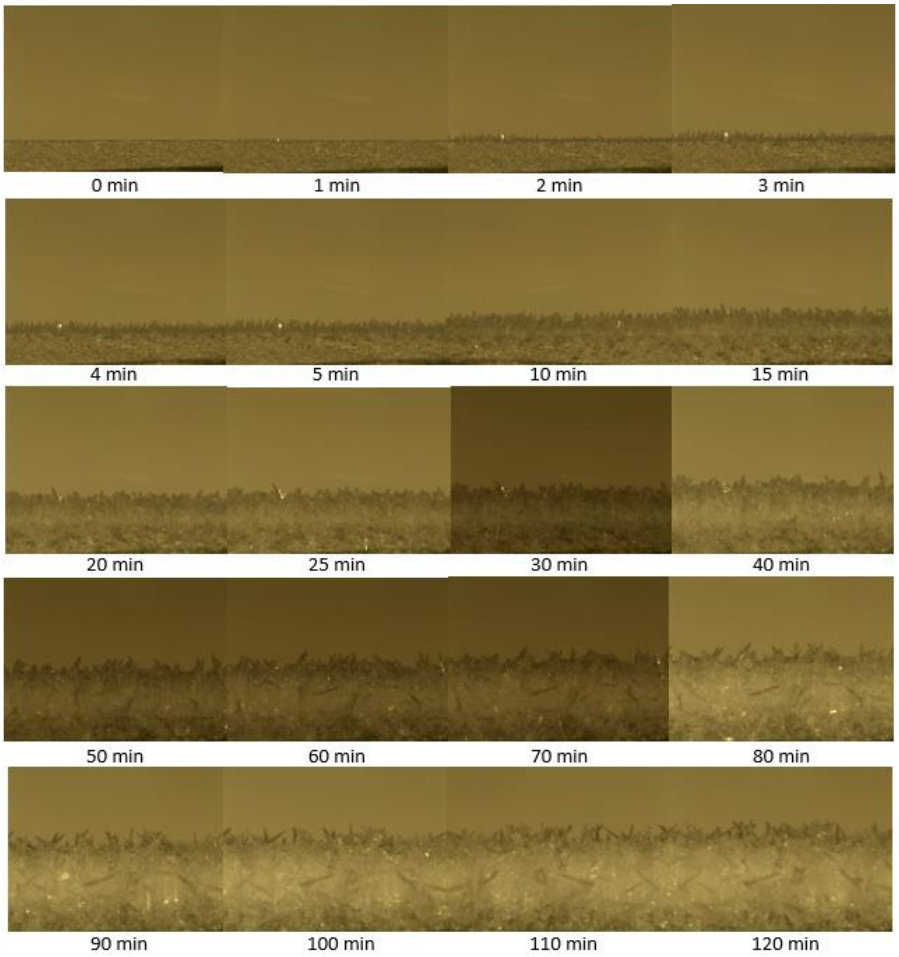

Figure 4: Pictures of the test section during frost accretion (test run no. 60)

3. DATA REDUCTION MODEL

The model proposed by Hermes et al. (2018) and validated by Sommers et al. (2018) for frost growth on hydrophilic and hydrophobic surfaces under natural convection conditions was used in the present study as the theoretical framework for data reduction. The model relies on the following assumptions: (i) quasi-static one-dimensional mass and heat diffusion; (ii) uniform frost layer along the flat plate, and (iii) the Lewis analogy is applicable. The model is derived from the overall mass balance in the frost layer combined with the following semi-empirical correlation for frost density, ρ_f, proposed by Hermes et al. (2014),

$$\frac{\rho_f}{\rho_i} = CJa^{-n}\sqrt{t} \tag{1}$$

where ρ_i is the density of ice, C can be a constant or a function of contact angle and relative humidity, and $Ja=c_p(T_{sat,a}-T_w)/(\omega_a-\omega_{sat,w})i_{sv}$ is the modified Jakob number, which represents the ratio between the sensible and the latent heat involved in the phase change process, and t stands for time. After some algebraic manipulations (see Hermes et al., 2018), the following algebraic expression for the time evolution of the frost thickness, δ, is achieved:

$$\delta = \frac{m}{\rho_i CJa^{-n}}\sqrt{t} + \frac{b}{\sqrt{t}} \tag{2}$$

where b is an integration constant, and m is the mass flux of water vapor into the frost layer.

Figure 5 illustrates equation (3), where one can see the two asymptotes in the time domain, one related to the first term ($\sim t^{1/2}$) and another based on the second term ($\sim t^{-1/2}$). The former stands for the frost growth over time while the latter can be associated with the frost decay. However, it is not possible on thermodynamic grounds to have a frost decay with a positive mass flux, meaning that eq. (3) can only be applied from the time when $d\delta/dt=0$ on.

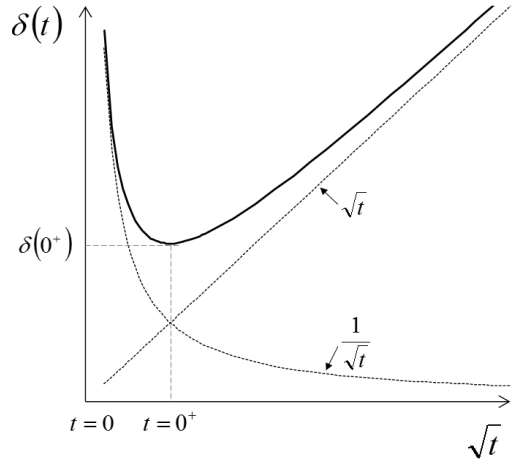

Figure 5: Illustration of the asymptotic behavior of equation (5) (Hermes et al., 2018)

In order to process the experimental results, eq. (2) was multiplied by $t^{1/2}$, yielding

$$\delta\sqrt{t} = at + b \tag{3}$$

where $a=m/\rho_i CJa^{-n}$ is constant over time (Negrelli et al., 2015). The coefficients a and b were reduced fitted each of 69 test runs – each comprising 12 experimental points with frost thickness varying over time – where it was observed that the variances (R^2) of the linear fits were above 0.99 for most of the test runs (66 out of 69), thus confirming the linearity between δ and $t^{1/2}$ predicted by the model. Those three data points have been dropped out from the following data analysis, which was carried out based upon the coefficients a and b of eq. (3), the first (slope) indicating the frost growth rate and the second (intercept) informing the initial condition of the process. In total, the analysis was performed considering 792 (66 x 12) data points.

4. RESULTS AND DISCUSSION

The sensitivity analysis was conducted by multivariable 1st order (linear) fits of the response variables (i.e., coefficients a and b) as functions of the independent variables (Montgomery, 2009), such as supercooling and supersaturation degrees, contact angle, air velocity, and air and surface temperatures, as follows:

$$\hat{a} = \alpha_0 + \alpha_1\Delta\omega + \alpha_2\Delta T + \alpha_3 V + \alpha_4 T_w + \alpha_5 T_a + \alpha_6\theta \tag{4}$$

$$b = \beta_0 + \beta_1\Delta\omega + \beta_2\Delta T + \beta_3 V + \beta_4 T_w + \beta_5 T_a + \beta_6\theta \tag{5}$$

In all cases, dimensionless forms of the response and independent variables were adopted, being calculated from

$$y = \frac{y - \frac{1}{2}\left(y_{max} + y_{min}\right)}{\frac{1}{2}\left(y_{max} - y_{min}\right)} \tag{6}$$

where ^ indicates a dimensionless value, varying in the interval [-1,1], and y_{max} and y_{min} the thresholds of the interval. The α and β coefficients obtained from the fittings of a and b, which express the sensitivity of the response variables to the independent ones, are reported in Fig. 6. It should be noted that the coefficients greater than unity (or lesser ones) are due to the confounding structure of the fit, which was limited to 1st order terms.

Figure 6.α reports the results obtained for the coefficient a as a function of the operating conditions, showing a great influence of the degree of supercooling, followed by the moderate influence of the surface temperature and degree of super-saturation. In general, little influence of contact angle and velocity on the growth rate is perceived. Figure 6.β depicts the results obtained for the coefficient b as a function of the operating conditions. Again, little influence of contact angle and velocity on coefficient b is observed, while the super-saturation and supercooling degrees were the most influential parameters, followed by the surface temperature with moderate effects. Effects of the same order were achieved for the super-saturation and the supercooling, which play equivalent roles on the nucleation process (Piucco et al., 2008), confirming the hypothesis that coefficient b carries information about the nucleation process, since it originates from the initial condition of the problem (Hermes et al., 2018).

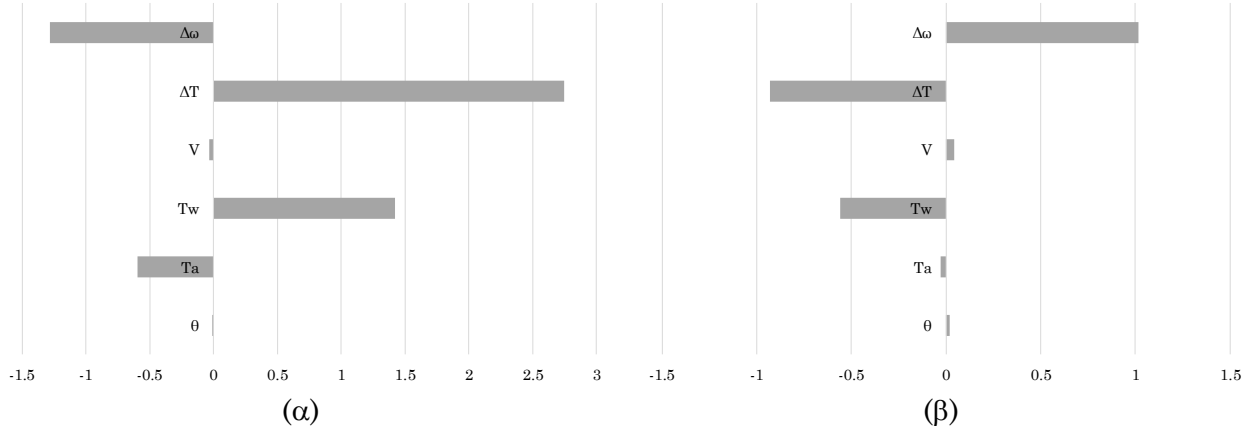

Figure 6: Sensitivity analysis of a and b with respect to the supercooling (ΔT) and the supersaturation (Δω) degrees, the air velocity (V), the air (T_a) and the surface temperatures (T_w), and the contact angle (θ)

Figure 7 shows the variation of b with the degree of supercooling, where a spreading of the data is observed when compared to a linear trend. Both positive and negative values for coefficient b can be noted. The former (b>0) can be associated with an early nucleation, before starting the time count in the test, which occurs by the presence of moist air between the cooled surface and the plastic film that is removed at time t=0. Since nucleation has already occurred for t<0, a positive frost thickness is observed at t=0. In the case of b<0, on the other hand, a late nucleation is likely to take place, since positive values δ are found only for t>0. Such a behavior is illustrated in Fig. 8.

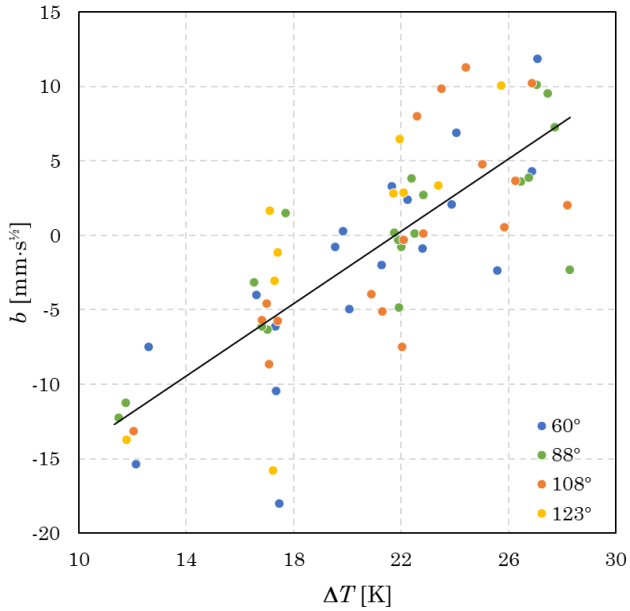

Figure 7: Variation of coefficient b with the supercooling degree for various contact angles

Moreover, one can see that the change of sign experienced by coefficient b takes place for a supercooling degree of 22 K, below which there is a delay in nucleation (b<0) and above which an early nucleation is observed (b>0), i.e. before removing the plastic film. In Fig. 7, the contact angles are represented by different colors, showing a random behavior without predominance of the hydrophobic surface (123°) in the region where there was delay in nucleation (b<0), and without predominance of the hydrophilic (60°) in the region where there was early nucleation (b>0). The scattering of the datapoints over a wide range of degrees of supercooling is an indication that the different contact angles did not influence the nucleation process and so the frost growth process as shown in Fig. 7. A possible explanation relies on the surfaces' roughness reported in Table 3, as rough surfaces generate sites suitable for nucleation, standing out the effect of the contact angle.

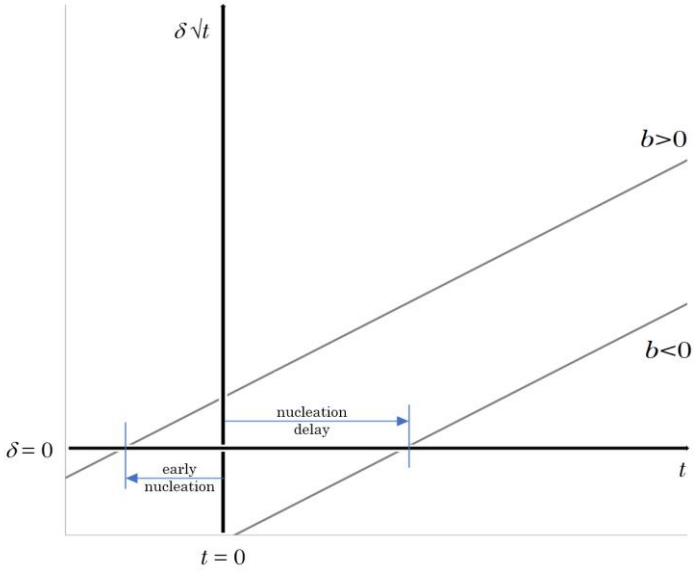

Figure 8: Physical interpretation of the sign of coefficient b

Noting that both a and b coefficients depend on the supercooling degree, the following modification in eq. (2) was provided so that a>0 always, whereas the sing of b can be positive or negative,

$$\delta = c_1 \Delta T^n \sqrt{t} + \frac{c_2 + c_3 \Delta T}{\sqrt{t}} \tag{7}$$

where $\Delta T \approx T_a - T_w$, and four parameters are to be fitted against all 792 experimental data points, providing n=3/4, c_1=0.00367, c_2=2/3 and c_3=-16.75, this being the set of coefficients that best represented the experimental data. Figure 9 compares the model results against the experimental data, where a good agreement can be observed, with 710 out of 792 points (90%) within the ±15% error bounds. The model is applicable to a range of supercooling degrees ranging from 12 to 28K and contact angles from 60 to 123°. The shades in greyscale mark data points from different test runs.

4. FINAL REMARKS

An experimental study on frost build-up on isothermal horizontal surfaces under forced flow conditions was presented. A purpose-built experimental apparatus was developed, which consists of a closed-loop wind-tunnel capable of controlling the velocity and psychrometric state of the air, and the temperature of the substrate. Different test surfaces were manufactured with a significant contact angles span, ranging from 60 to 123°. An image acquisition system was used to measure the thickness of the frost during the tests for supercooling degrees ranging from 10 to 30K. From the experimental apparatus, 69 experimental runs were performed – each providing 12 datapoints for the frost thickness over time, totalizing 828 experimental points – varying the air temperature, humidity and velocity, the surface temperature and the surface contact angle.

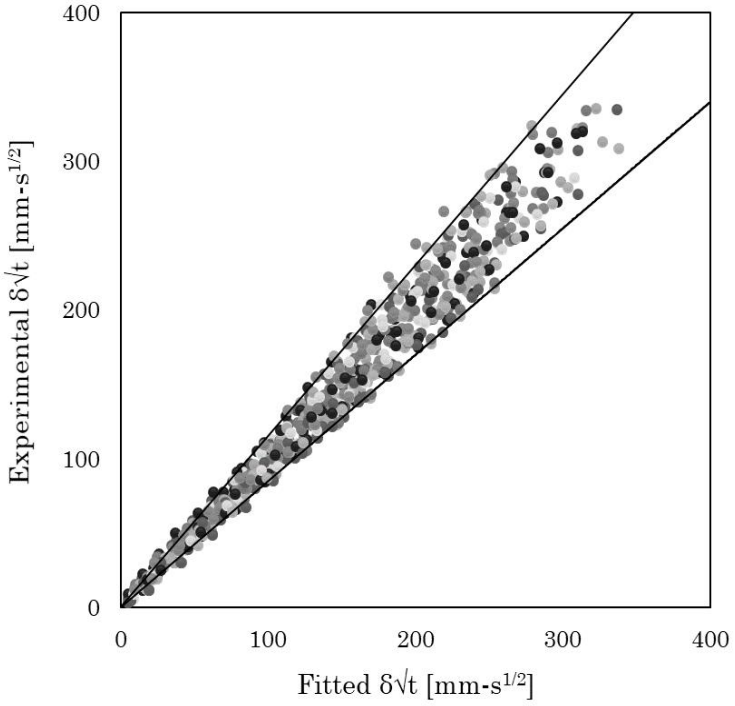

Figure 9: Comparison between the experimental frost thickness data and the results of eq. (7)

The analysis of the data was performed based on the coefficients a and b of the linear relation $\delta\sqrt{t}=at+b$, derived from a theoretical model advanced in a prior publication, which correlated quite well a great majority of the experimental dataset (68 out of 69 runs with $R^2>0.99$). The coefficient a, which expresses the frost growth rate, and coefficient b, which is supposed to convey the influence of the initial conditions to the model, have both shown to be less influenced by the contact angle and air velocity, albeit highly affected by factors as surface temperature and supercooling degree. Both positive and negative values were achieved for coefficient b, the former associated with early nucleation, before starting of time count during the tests, which occurs because of the presence of moist air between the cooled surface and the plastic film at time t=0. On the other hand, a delay in the nucleation process can be observed for negative b values. No expected influence of the contact angle on the onset of nucleation was observed. A possible explanation is associated with the roughness of the surface, where rough surfaces generate nucleation sites, surpassing the effect of the contact angle.

NOMENCLATURE

Roman

a,b	coefficients of eq. (3)
C	constant of eq. (1)
$c_1…c_3$	coefficients of eq. (7)
c_p	specific heat of moist air [J kg^{-1}K^{-1}]
i_{sv}	latent heat of sublimation [J kg^{-1}]
Ja	modified Jakob number [-]
m	mass flux [kg m^{-2} s^{-1}]
n	exponent of eq. (3)
T	temperature [K]
t	time [s]

Greek

$\alpha_0…\alpha_6$	coefficients of eq. (4)
$\beta_0…\beta_6$	coefficients of eq. (5)
δ	frost thickness [m]
ΔT	supercooling degree [K]
$\Delta\omega$	supersaturation degree [-]
ρ	frost density [kg m^{-3}]
ω	humidity ratio [-]

Subscripts

a	moist air
f	frost
max	maximum
min	minimum
sat	saturated
w	wall

REFERENCES

Farhadi S, Farzaneh M, Kulinich SA, Anti-icing performance of superhydrophobic surfaces, Applied Surface Science, 257 (2011), 6264-6269

Hermes CJ, Loyola FR, Nascimento Jr VS, A semi-empirical correlation for the frost density, Int. J. Refrig. 46 (2014), 100-104

Hermes CJL, Sommers AD, Gebhart CW, Nascimento VS, A semi-empirical model for predicting the frost accretion on hydrophilic and hydrophobic surfaces, Int. J. Refrig. (2018) doi.org/10.1016/j.ijrefrig.2017.09.022

Jhee S, Lee KS, Kim WS, Effect of surface treatments on the frosting/defrosting behavior of a fin-tube heat exchanger, Int. J. Refrig. 25 (2002) 1047–1053

Kim K, Lee, K-S, Frosting and defrosting characteristics of a fin according to surface contact angle, Int. J. Heat Mass Transfer 54 (2011), 2758-2764

Kim M-H, Kim H, Lee K-S, Kim D-R, Frosting characteristics on hydrophobic and superhydrophobic surfaces: A review, Energy Conversion and Management 138 (2017) 1–11

Lee H, Shin J, Ha S, Choi B, Lee J. Frost formation on a plate with different surface hydrophilicity, Int. J. Heat Mass Transfer 47 (2004) 4881-4893.

Liu Z, Wang H, Zhang X, Meng S, Ma C, An experimental study on minimizing frost deposition on a cold surface under natural convection conditions by use of a novel anti-frosting paint. Part I. Anti-frosting performance and comparison with the uncoated metallic surface, Int. J. Refrig. 29 (2006) 229-236

Montgomery DC (2017) Design and analysis of experiments, Wiley

Negrelli S, Nascimento Jr VS, Hermes CJ, A study of the effective thermal conductivity of frost formed on parallel plate channels, Exp. Therm. Fluid Sci. 78 (2016), 301-308

Piucco RO, Hermes CJ, Melo C, Barbosa Jr JR, A study of frost nucleation on flat surfaces, Exp. Therm. Fluid Sci. 32 (2008), 1710-1715

Rahimi M, Afshari A, Fojan P, Gurevich L, The effect of surface modification on initial ice formation on aluminum surfaces, Applied Surface Science 355 (2015), 327-333

Ribeiro RS, Hermes CJL, Silva DL, Thermal-Hydraulic Optimization of Fan-Supplied Tube-Fin Evaporators for Frosting Conditions Aiming at Minimum Energy Consumption, 17th Int. Refrig. and Air Cond. Conf. at Purdue, 2018, West Lafayette-IN, USA, Paper 2113

Silva DL, Hermes CJL, Defrost Cycle Optimization for Fan-Supplied Tube-Fin Evaporators Subjected to Frosting Conditions, 17th Int. Refrig. and Air Cond. Conf. at Purdue, 2018, West Lafayette-IN, USA, Paper 2107

Sommers AD, Gebhart CW, Hermes CJ, The role of surface wettability on natural convection frosting: Frost growth data and a new correlation for hydrophilic and hydrophobic surfaces, Int. J. Heat Mass Transf. 122 (2018), 78-88

Sommers AD, Napora AC, Truster NL, Caraballo EJ, Hermes CJ, A semi-empirical correlation for predicting the frost density on hydrophilic and hydrophobic substrates, Int. J. Refrig. 74 (2017), 313-323

Sommers AD, Truster NL, Napora AC, Riechman AC, Caraballo EJ ,Densification of frost on hydrophilic and hydrophobic substrates–Examining the effect of surface wettability, Exp. Therm. Fluid Sci. 75 (2016), 25-34

Song M, Dang C, Review on the measurement and calculation of frost characteristics, Int. J. Heat Mass Transfer 124 (2018) 586–614

Wang ZJ, Kwon DJ, DeVries KL, Park JM, Frost formation and anti-icing performance of a hydrophobic coating on aluminum, Exp. Therm. Fluid Sci. 60 (2015), 132-137

Wu X, Dai W, Shan X, Wang W, Tang L, Visual and theoretical analyses of the early stage of frost formation on cold surfaces, J. Enhanced Heat Transfer, 14 (2007), 257-268

ACKNOWLEDGEMENTS

The experimental work reported in the paper was carried out at the Federal University of Paraná with financial support from the Brazilian Government funding agencies CAPES and CNPq.